

# URBAN WIND FIELD GENERATION USING LES FOR APPLICATION TO QUADROTOR FLIGHT

Mark Sutherland\* , Jason Etele\*\*

\*MAsc Candidate, Carleton University , \*\* Associate Professor, Carleton University

**Keywords:** LES, Urban Environment, Quadrotor, UAV, Simulation

## Abstract

*This work proposes a method for generating urban wind fields using large-eddy simulation around discrete structures such as a single building or urban canyon. The wind velocity data is stored in a database and queried by a flight simulator to design and optimize autonomous control algorithms. A custom quadrotor TARA, with a motor to motor distance of approximately 0.4 m, uses PID position control to evaluate the position deviation at two locations in three background wind conditions. Position hold in the wake produces deviation spheres of radii 2.13, 5.67 and 13.38 body lengths with no wind, RANS wind and LES wind respectively. Position hold above the building roof produces deviation spheres with radii of 4.16, 10.44 and 18.80 body lengths before a building strike with LES wind. The LES wind results in a radius increase of up to 525% in comparison to no wind and up to a 135% increase for RANS wind.*

## 1 Introduction

The research, designing, building and utilization of unmanned aerial vehicles (UAVs) and micro aerial vehicles (MAVs) has dramatically increased over last decade. With 53% of the world's population living in an urban environment, and increasing 2% annually [1], there is little surprise in the growing interest to use UAVs and MAVs in urban environments. The interest is motivated by many mission profiles such as law enforcement [2], general reconnaissance and surveillance [3], human risk-reduction in military operations [4] or aerial photography for urban inspection [5]. A quadrotor is one potential UAV

which could be used to fulfill such missions due to its size, maneuverability and cost. While there has been significant research in the design and utilization of quadrotors, few studies account for the wind effects on fully autonomous flight in urban environments.

The flight performance in the urban environment is a concern due to the quadrotor's small size and light weight coupled with the fluctuating velocity fields around urban structures [6]. Knowledge of the fluctuating velocity fields is a result of the substantial research in general bluff body aerodynamics [7], scalar concentration dispersion in the form of pollutant dissemination [8], application of wind loading on buildings [9] and pedestrian comfort level in urban environments [10].

To study the effects of the wind on autonomous quadrotor control a flight simulator has been developed that incorporates urban wind fields generated using computational fluid dynamics (CFD)[11]. Even with the simplest CFD model and urban geometry the numerical simulations are unable to run in real time with the flight simulator. For this reason the wind velocity fields are generated before running the flight simulator, stored in a database and queried by the flight simulator as needed at runtime.

Previous simulation work consisted of using a Reynolds-Averaged Navier-Stokes (RANS) method to generate the urban wind field for testing a fixed wing Aerosonde UAV [12] and Yamaha R-50 rotorcraft [13]. This work expands the RANS database with a subset of flow fields suitable for testing a quadrotor with wind generated using a large-eddy simulation (LES) ap-

proach. This LES subset aims to better resolve the smaller turbulent motions in the buildings wake, as compared to a RANS simulation, challenging the flight controller with more realistic conditions.

This paper first outlines how an urban environment is parameterized as a series of smaller geometries. This is followed by a brief explanation of the LES model. The verification and validation of the flow field generated from a single square building is then presented. Finally this flow field and a RANS equivalent are used with the flight simulator to illustrate a quadrotor's flight performance.

## 2 Definition of the Urban Environment

While it can be advantageous to simulate an entire urban domain [14] to replicate as near realistic wind conditions as possible, several different urban scales need to be considered. The four length scales used in classifying urban environments are; regional (100-200 km), city (10-20 km), neighborhood (1-2 km) and street level (100-200 m) [15]. Since even the largest quadrotors have scales orders of magnitude lower than the street level, simulating on the city scale using grid elements required for a quadrotor would make it computationally expensive.

Therefore in order to reduce the size of a typical North American city to one which is computational feasible, the environment is broken into simplified geometries. These geometries are then assembled to replicate a given urban environment. The most basic geometric units are a single building in isolation and an urban canyon. The parametrization of a single building is achieved by three variables, the Reynolds number ( $Re_D$ ), the wind incidence angle ( $\theta_W$ ) and the ratio of the building length to width ( $L/W$ ). The Reynolds number is based on the characteristic length  $D$  illustrated in Figure 1,

$$Re_D = \frac{U_\infty D}{\nu} \quad (1)$$

where:

- $U_\infty$  is the free stream velocity
- $D = \sqrt{L^2 + W^2}$
- $\nu$  is the kinematic viscosity

An urban canyon geometry is formed due to the flow interactions not otherwise found with single building in isolation. One such interaction is the generation of a turbulent canyon vortex contained within the canyon street length. The urban canyon is parametrized with a set of characteristic length for each building with the addition of the street separation distance  $S$ , and a height differential  $\Delta H$ . The  $\Delta H$  shown in Figure 1 is negative by convention and classified as a step up notch.

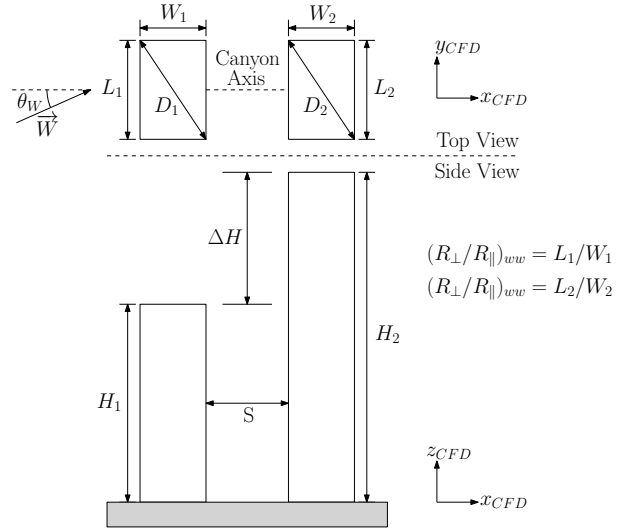


Fig. 1 Urban canyon parameters

The wind vector  $\vec{W}$  can be offset at a wind incidence angle  $\theta_W$  representing the buildings orientation with respect to the freestream wind. Previous work has shown this variable has a strong affect on the size and existence of certain turbulent flow structures around an urban structure. Only single building geometry is studied in this work with parameter of  $Re = 7.30 \times 10^6$ ,  $\theta_W = 0$  and  $(R_{\perp}/R_{\parallel})_{ww} = 1$ . Therefore by varying the non-dimensional parameters in the numerical simulations a variety of urban geometries and environments can be built up in the flight simulator by matching parameters.

## 3 LES modeling

The CFD package OpenFOAM is used to implement the LES used in this work. One of the fundamental differences between RANS and LES is the former averages the turbulent fluctuations in time while the latter averages them in space.

In general LES utilizes a low-pass filter to attenuate high frequency turbulent motions while leaving the low frequency motions unaltered. This is performed by applying a spatial filter as a function of a filter scale  $\Delta$  to the flow variables. The filtering process on the velocity takes the form of:

$$\bar{u}(x, t) = \int G(r, x, \Delta) u(x - r, t) dr \quad (2)$$

where:

- $G$  is a filter function
- $u$  is the original unfiltered velocity
- $\bar{u}$  is the filtered velocity
- $r$  is a cell local axis

The small scale motions are removed but their affect on the flow is grouped into a sub-grid scale (SGS) residual [16]. The original velocity field is then decomposed into filtered ( $\bar{u}$ ) and subgrid-scale ( $u'$ ) velocity components,

$$u(x, t) = \bar{u}(x, t) + u'(x, t) \quad (3)$$

The filter width is comparable to the resolved filtered eddies and on the order of the grid for finite volume CFD methods. Since there is no benefit to specifying a filter width smaller than the grid size, the most accepted method of defining the filter width is to use the cube root of the cell volume [17],

$$\Delta = \sqrt[3]{\Delta_x \Delta_y \Delta_z} \quad (4)$$

While there are several options of filter functions, when using a finite volume method the Top-hat or box filter is most commonly used,

$$G(x, \Delta) = \begin{cases} 1/\Delta & : |x - r| \leq \Delta/2 \\ 0 & : otherwise \end{cases} \quad (5)$$

Since the flow variables are piecewise linear functions of  $x$  and a box filter is simply a spatial average over a region, by making the filter width equal to the grid spacing, the filter average is simply the local average [18]. After the decomposition of equation 3 is substituted into the unsteady incompressible Navier-Stokes equations and the filtering is applied, the governing equations of motion for LES are given by:

$$\frac{\partial \bar{u}_i}{\partial x_i} = 0 \quad (6)$$

$$\frac{\partial \bar{u}_i}{\partial t} + \frac{\partial}{\partial x_j} (\bar{u}_i \bar{u}_j) = -\frac{1}{\rho} \frac{\partial \bar{p}}{\partial x_i} + \frac{\partial}{\partial x_j} \left( \nu \frac{\partial \bar{u}_i}{\partial x_j} \right) \quad (7)$$

This produces a non-linear convection term  $\bar{u}_i \bar{u}_j$  which is not a function of known flow variables,  $\bar{u}$  or  $u'$  but rather  $\bar{\bar{u}}$  and  $\bar{u}'$ . Since  $\bar{\bar{u}} \neq \bar{u}$  and  $\bar{u}' \neq 0$ , Leonard's decomposition is applied to group these terms into a single SGS tensor:

$$\tau_{ij} = \bar{u}_i \bar{u}_j - \bar{\bar{u}}_i \bar{u}_j \quad (8)$$

Making the substitution of equation (8) into equation (7) the filtered momentum equations becomes:

$$\frac{\partial \bar{u}_i}{\partial t} + \bar{u}_j \frac{\partial \bar{u}_i}{\partial x_j} = -\frac{1}{\rho} \frac{\partial \bar{p}}{\partial x_i} + \frac{\partial}{\partial x_j} \left( \nu \frac{\partial \bar{u}_i}{\partial x_j} \right) - \frac{\tau_{ij}}{\Delta x_j} \quad (9)$$

To close Equations (6) and (9) a model is applied to relate the SGS stress tensor to known flow quantities. Using the Boussinesq eddy viscosity assumption, the SGS stress tensor is proportional to the local filtered rate of strain tensor and SGS viscosity.

$$\tau_{ij} = -2\nu_{SGS} \bar{S}_{ij} + \frac{1}{3} \tau_{kk} \delta_{ij} \quad (10)$$

where  $\bar{S}_{ij} = \frac{1}{2} \left( \frac{\partial \bar{U}_i}{\partial x_j} + \frac{\partial \bar{U}_j}{\partial x_i} \right)$  and  $\delta_{ij}$  is the Kronecker delta. The complementary spherical tensor  $\tau_{kk}$  is grouped in with the filtered pressure term and therefore does not require additional modeling.

There are several models to relate the SGS viscosity to known flow parameters. The one equation eddy SGS model was selected as it overcomes the equilibrium assumption of the Smagorinsky model [18]. It also posses the ability to predict backscatter and has higher numerical stability making it computationally easier than the older dynamic Smagorinsky model [19].

$$\nu_{SGS} = C_k \Delta \sqrt{k_{SGS}} \quad (11)$$

The one equation eddy model relates the SGS viscosity through a characteristic length scale and a SGS velocity scale. To incorporate the changes

of this SGS velocity scale a SGS turbulent kinetic energy transport equation is also defined:

$$\frac{\partial k_{SGS}}{\partial t} + \frac{\partial(k_{SGS} \bar{u}_j)}{\partial x_j} = \frac{\partial}{\partial x_j} \left[ (v_{SGS} + v) \frac{\partial k_{SGS}}{\partial x_j} \right] + \tau_{ij} \bar{S}_{ij} - \epsilon_{SGS} \quad (12)$$

where  $\epsilon_{SGS} = C_\epsilon (k_{SGS}^{3/2}/\Delta)$ ,  $C_k = 0.094$  and  $C_\epsilon = 1.048$ .

#### 4 Computational Domain and Grid

The domain shown in Figure 2 is generated to follow the standards outlined in the COST Action 732 [20] and the Agriculture Institute of Japan (AIJ) guidelines [21] to achieve the proper blockage ratios, boundary conditions and initial grid sizing. The overall domain is made large enough to allow for specification of free slip boundary conditions where possible, saving computational power in terms of required cell refinement and application of wall functions.

The mapped inlet boundary condition is generated by sampling the resolved velocity component at a plane 12 building widths downstream from the inlet, and scaling it to ensure the bulk flow rate or inlet flux is constant on the inlet plane [18]. The outlet is a zero gauge pressure outlet. OpenFOAM employs the universal velocity profile wall functions based on Spalding's law [18]. The advantage of this wall function is its scalability to allow for the first grid point to be in a variety of regions without changing the wall function model. These wall functions are applied to the building and ground to greatly reduce the required grid size at the no slip surfaces.

The grids used are generated with OpenFOAM native mesher snappyHexMesh which produces a Cartesian hexahedra grid or multi-grid. Local grid refinement is used to allow for the overall domain size to be large enough to mitigate the affects of the boundary conditions, while still having a cell size allowing the simulation to have wind data at points spaced on the order of the size of a quadrotor. While local refinement helps reduce computational cost it

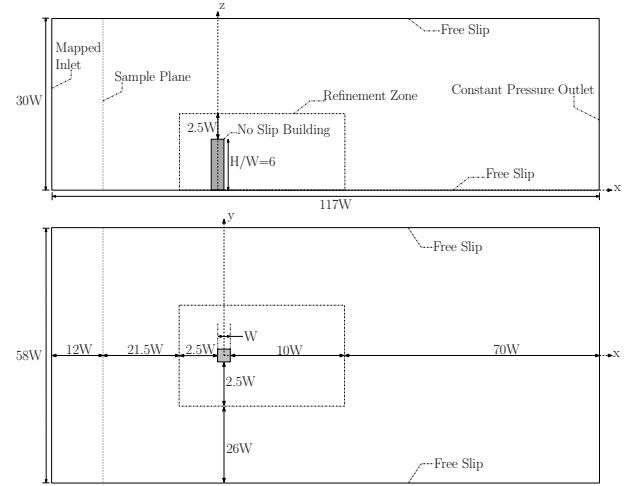


**Fig. 2** Computational domain, boundary conditions and local refinement zone definition.

generates commutation error at the boundaries as well as changes the resolved scales filter width as defined in equations (4) and (5) [18]. To allow the errors to naturally dissipate in the flow, the refinement boundaries are placed far from the area of interest with gradual steps in refinement to prevent large instantaneous changes to the filter width as shown in Figure 3.

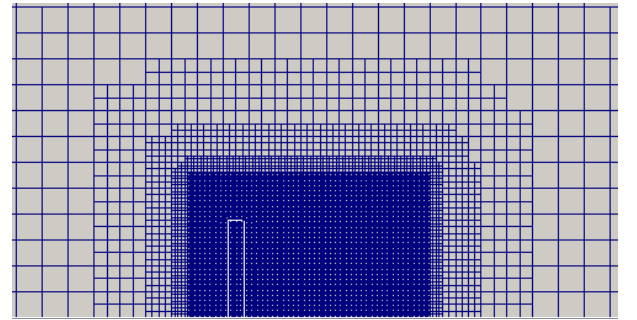


**Fig. 3** Cartesian hex mesh with gradual cell refinement

Three computational grids are used to validate the flow field in Section 6. The only variable between grids is the number of cells on the building thus increasing the spatial resolution in the buildings wake.

The coarsest grid has 10 nodes per building side ( $W$ ), and is refined 1.5 times in each direction on subsequent refinements in mesh size. Table 1 summarizes the total cell count and computational time of the three validation grids.

**Table 1** Refined area grid details

Name	# building cells	Total # cells	CPU Hours
Coarse	10x10x60	$1.13 \times 10^6$	0.838
Medium	15x15x90	$2.43 \times 10^6$	3.383
Fine	22x22x132	$7.67 \times 10^6$	17.696

### 5 Numerical Procedure

To generate an initial velocity field a potential flow solver is used. This velocity field is then used as an initial solution to a steady RANS  $k - \omega$  SST simulation. The RANS simulation is performed to provide the LES with an initial turbulent velocity field in order to decrease the start up time of the LES flow. Both simulations are based on the finite volume approach where the RANS is solved with the Semi-Implicit Method for Pressure-Linked Equations (SIMPLE) method and LES with the Pressure Implicit with Splitting of Operators (PISO) method [17].

The LES timestep is varied between the different grid sizes to ensure the Courant-Friedrichs-Lewy (CFL) number is maintained within a range of 0.4-0.6 in the most refined region. To compare the LES results to those of experiments and previous RANS simulations the velocity field is time averaged over an average window. As outlined in Table 2 the LES is performed for 30 seconds and the time averaging for 24 seconds. The averaging is initiated after the first 6 seconds to allow the mapped flow field of the steady RANS results to transition into flow with coherent vortical structures.

**Table 2 Numerical details**

Pressure-velocity coupling algorithm	PISO
Time discretization	Second order
Spatial discretization	Central difference
Time step	$8 \times 10^{-4}$ s
Total simulation time	30 s
Average window	24 s
Loop interval	18.6 s

To minimize the required LES computational time the flow is studied for periodic patterns to allow for repetitive use of wind velocity over a loop interval. The data in the loop interval is stored in a database and repeatably called for flight simulations longer than the interval. The loop interval is found using a space fixed probe at  $x/W = 2$ ,  $y/W = 0$ , and  $z/H = 0.625$  and visual inspections of velocity contour plots.

The filtered spanwise velocity ( $\bar{v}$ ) at the probe is shown in Figure 4 which displays a sinusoidal like pattern. This increasing and decreasing velocity cycle is due to the bulk of the large motions oscillating in along the  $y$  axis over time. The repetition interval stored in the database has a period

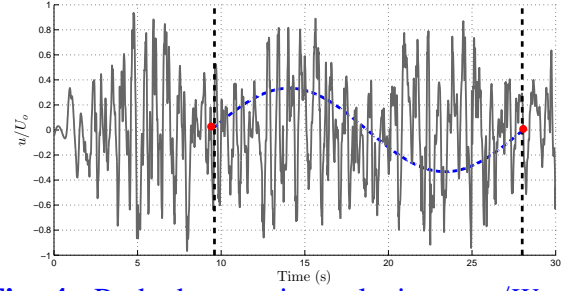


**Fig. 4** Probed spanwise velocity at  $x/W = 2$ ,  $y/W = 0$ , and  $z/H = 0.625$

of approximately 18 seconds, includes two maximums to allow for a full wake deflection in both direction. Suitable start and end times are found from data points near the repetition interval lines in Figure 4 (9.4 and 28.0 seconds), with velocities close to 0 m/s and have similar velocity gradients. This is done to minimize a discontinuity between the end and start of loop intervals.

### 6 Verification and Validation

Since the grid size is directly proportional to the filter width and resolved scales, additional grid independence techniques are required when compared to a similar RANS simulation. LES verification is first required to ensure the numerical results follow the guidelines and definitions of LES flow. This is followed by the numerical validation against experimental data to check if the flow field is physical in nature. Verification and validation comparisons are performed along the  $1.25W$  measurement line shown in Figure 5, based on a subset from flow experiments around a 1:1:2 ratio highrise in the work of Meng and Hibi [22]. Figure 5 also shows the probe location at which the data in Figure 4 is obtained.

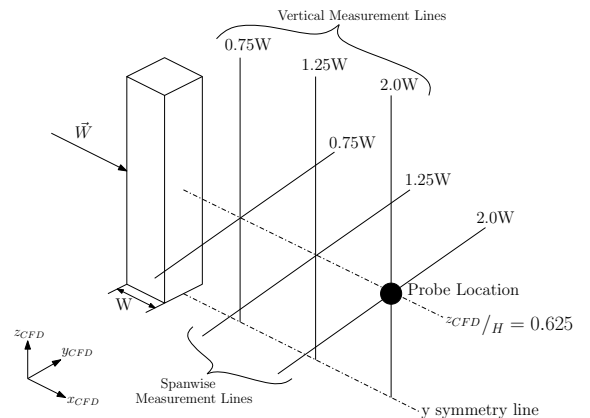


**Fig. 5** Measurement sample locations

## 6.1 LES Verification

Numerous verification techniques have been proposed for the verification of LES such as; two point correlations,  $LES\_IQ_k$ , the ratios of SGS viscosity to total viscosity, the ratio of SGS stress to total stress, and Systematic Grid and Model Variation (SGMV). While it has been shown two point correlations are the most useful method in evaluating the adequacy of grid resolution, they require substantial post processing time [23]. In this work the index quality based on the resolved turbulent kinetic energy ( $LES\_IQ_k$  [24]) is used. The turbulent kinetic energy (TKE) index quality is defined as:

$$LES\_IQ_k = \frac{k^{res}}{k^{tot}} = 1 - \frac{|k^{tot} - k^{res}|}{k^{tot}} \quad (13)$$

where:

- $k^{res}$  is the LES resolved TKE
- $k^{tot}$  is the theoretical max resolvable TKE

Therefore, the index quality ratio is 1 when all energy and motion scales are directly resolved. As LES filters out the TKE at high wavenumbers this ratio decreases. The flow is considered high quality LES when 80% of the TKE is resolved and  $LES\_IQ_k \geq 0.8$  [16, 24]. The difficulty lies in obtaining the total TKE ( $k^{tot}$ ) without performing DNS or detailed experimental results. However using the results of two LES on different grid sizes and a Richardson extrapolation one can approximate the TKE that would be resolved with an infinite number of cells. The extrapolation constant is found from:

$$a_k = \frac{1}{h_2^p} \left[ \frac{k_2^{res} - k_1^{res}}{(h_1/h_2)^p - 1} \right] \quad (14)$$

where:

- $k_1^{res}$  is the resolved TKE on grid 1
- $k_2^{res}$  is the resolved TKE on grid 2
- $h_i$  is the characteristic grid quality
- $p$  is the order of numerical accuracy

For a finite volume solving method the characteristic grid quality  $h_i$  is taken as the square root of the cell volume, or the filter width ( $h_i = \sqrt[3]{V} = \Delta$ ). The order of numerical accuracy for

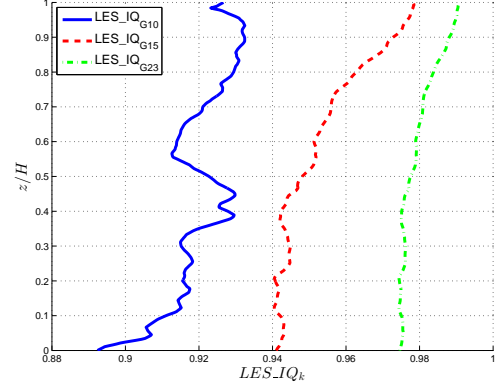


Fig. 6  $LES\_IQ_k$  at  $x/W = 1.25$ ,  $t=30$

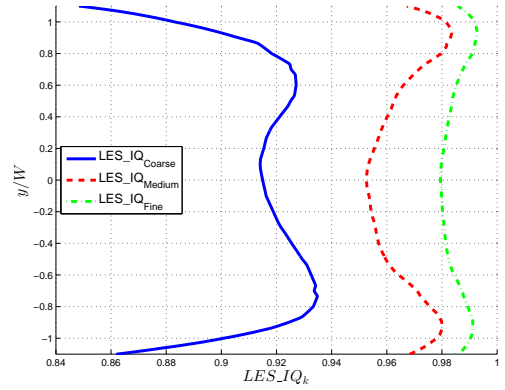


Fig. 7 Spanwise  $LES\_IQ_k$  at  $x/W = 1.25$ ,  $t=30$

this study  $p$  is second order accurate ( $p = 2$ ). With the extrapolation constant ( $a_k$ ) determined, a quality indices can be defined for the TKE resolved on each grid:

$$LES\_IQ_k^1 = 1 - \frac{|a_k h_1^p|}{k_1^{res} + a_k h_1^p} \quad (15)$$

$$LES\_IQ_k^2 = 1 - \frac{|a_k h_2^p|}{k_2^{res} + a_k h_2^p} \quad (16)$$

where:

- $LES\_IQ_k^1$  is the quality index of grid 1
- $LES\_IQ_k^2$  is the quality index of grid 2

Therefore a quality index is generated for both of the grids used in one extrapolation. This results in a total of four incidences where the second index of the first extrapolation is equal to the first index of the second extrapolation. The calculated index quality along the  $1.25W$  vertical and horizontal measurement lines are shown in Figures 6 and 7 and it is seen that even the coarsest grid resolves more than 80% of the TKE. The sharp drop off at  $y = \pm 1$  in Figure 7 is a result of

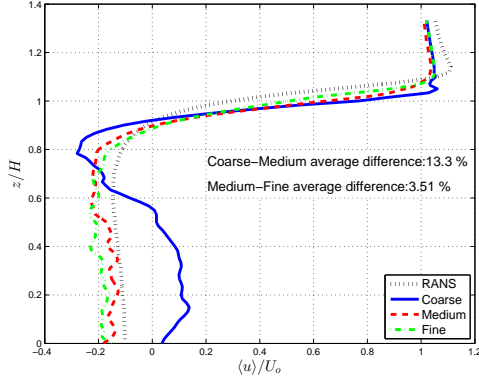


**Fig. 8** Time averaged streamwise velocity profile comparison along vertical line at  $x/W = 1.25$

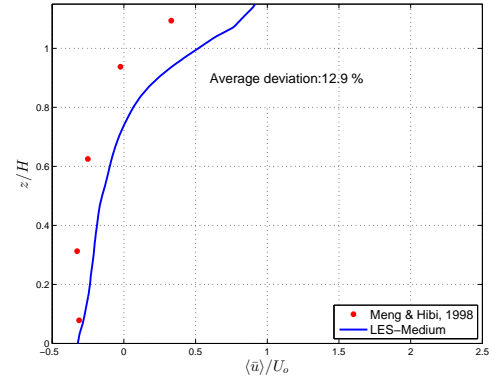


**Fig. 10** Time averaged streamwise velocity profile along vertical line at  $x/W = 1.25$

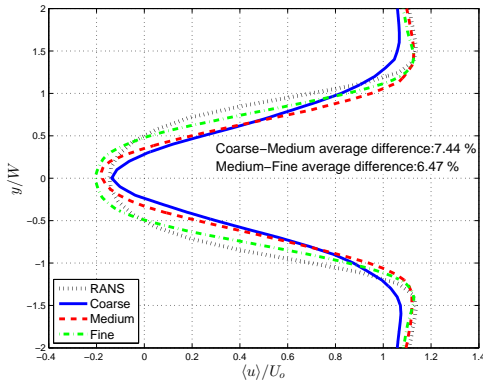


**Fig. 9** Time averaged streamwise velocity profile comparison along spanwise line at  $x/W = 1.25$

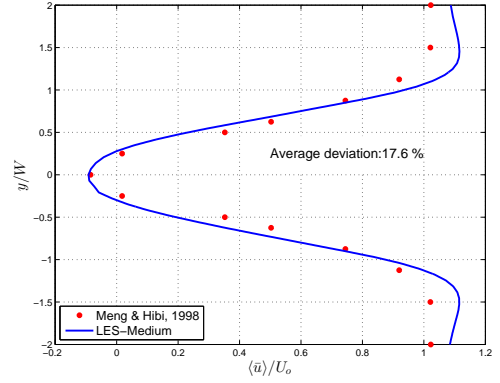


**Fig. 11** Time averaged streamwise velocity profile along spanwise line at  $x/W = 1.25$

the reduced turbulent motion and energy outside of the building wake.

An additional verification is performed by comparing the time averaged streamwise velocity profiles (shown in Figures 8 and 9). The average difference in the velocity from the coarse to medium grid and medium to fine grid is also calculated and shows a decreasing trend along the both measurement lines. Therefore the medium grid is used for all wind generating simulations.

## 6.2 LES Validation

Using the medium grid the time averaged streamwise velocity profiles of the LES are compared to the experimental results from Meng and Hibi [22]. The wind tunnel experiments consist of flow past a scaled 1:1:2 high-rise building with an atmospheric boundary layer (ABL) velocity profile at the inlet resulting in a Reynolds number of  $Re_H = 2.40 \times 10^4$ . It is found that the inlet velocity profile has minimal affect on the velocity in the building wake and thus a uniform inlet as outlined in section 4 is used.

The experimental and numerical velocities along the vertical and spanwise measurement lines are shown in Figures 10 and 11. Calculating an average deviation between the LES and experimental points yields a difference of 12.9% in the vertical direction and 17.6% in the horizontal direction at a length of  $1.25W$  downstream of the building.

## 7 Simulator Implementation

The TARA quadrotor is a custom airframe and autopilot with an operational weight of 2.2 kg and motor to motor distance of 428 mm. The autopilot control loops and quadrotor dynamics are estimated in MATLAB and Simulink for the purpose of flight simulation [25].

TARA currently uses two PID controllers to stabilize the quadrotor attitude and maintain a desired position. The forces resulting from the wind velocity components as found from the LES database are applied to the center of gravity (CG) when calculating the vehicle flight performance.

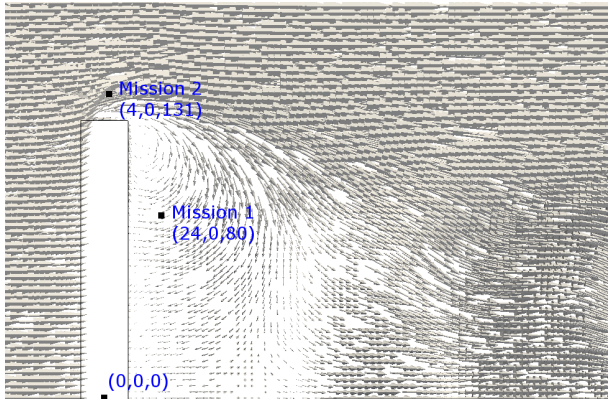


Fig. 12 Midplane RANS wind vectors at  $t=18.6$  s

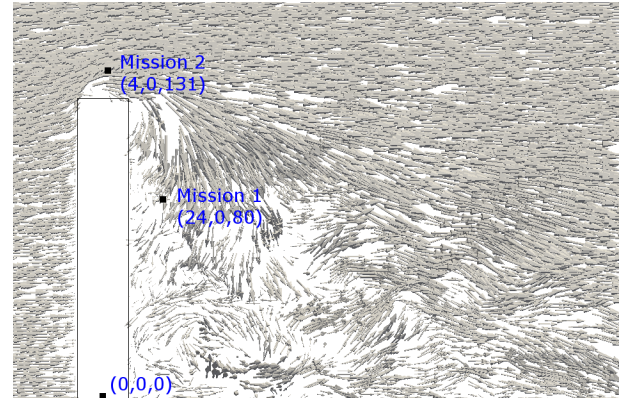


Fig. 13 Midplane LES wind vectors at  $t=18.6$  s

### 8 Position Hold Results

To study the performance of autonomous navigation with wind gusts, a single building geometry is tested with no wind, RANS generated wind based on previous work [12, 13], and LES generated wind. The wind simulations use the average wind speed in a Canadian urban city of 4 m/s [26] resulting in building dimensions of 20 m x 20 m x 120 m to match the Reynolds number of that used in the CFD simulations.

Two position hold missions are performed at locations where the resulting wind velocities and motions would provide a challenge for the position controller. Mission 1 is in the turbulent building wake, highly influenced by the downward flow over the top of the building. Mission 2 is in a region of highly accelerated flow over the buildings roof where the velocity is approximately 33% faster than the 4 m/s freestream. Both mission positions are superimposed on the RANS and LES wind fields from the database at  $t=18.6$  seconds in Figures 12, and 13.

The maximum and minimum position deviations of each axis are shown in the X-Y and X-Z planes in Figures 14 and 15 for each mission. The desired over point, the position of the buildings and its size is also shown.

**Table 3** Radius of equivalent position deviation spheres relative to TARA body length

	No Wind	RANS	LES
Mission 1	2.13	5.67	13.38
Mission 2	4.16	10.44	18.80

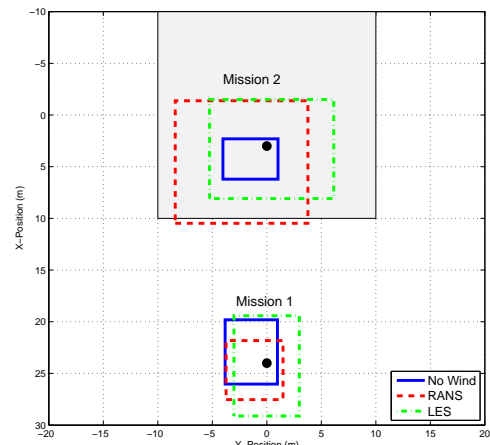


Fig. 14 Mission 1 and 2 X-Y deviation areas

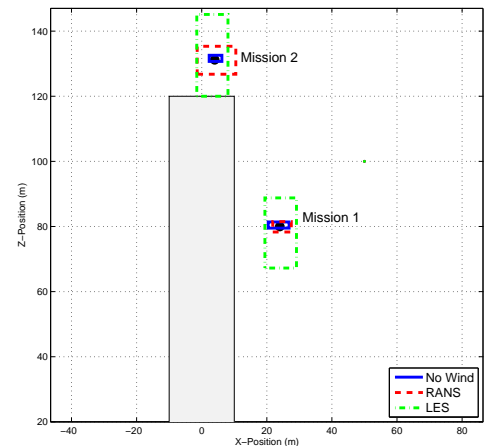


Fig. 15 Mission 1 and 2 X-Z deviation areas

Table 3 summarizes the radius in TARA body lengths of a sphere of equivalent volume to approximate the position deviations under each wind condition. While the RANS wind increased the position deviation radius by 166% in Mission 1, the LES wind produced a much larger error volume resulting in a 528% and 135% ra-

dial increase compared to the no wind and RANS wind respectively. This increase is due to the strong time varying downward wind force which induces oscillations as the strong wind fluctuations are periodically applied to the quadrotor and the controller continually attempts to recover.

While the RANS and LES X-Y position deviations (Figure 14) are similar in Mission 2, the transient flapping of the flow over the sharp building edge produces a much larger Z deviation (Figure 15) with LES wind. The body length radius increases by 151% when comparing the no wind and RANS wind volumes. The radial increase when using no wind to LES wind is 351% and 80% between RANS and LES wind. Additionally the controller is unable to hold position with the LES wind in Mission 2 and strikes the building after 87.12 seconds.

## 9 Summary and Conclusions

In the present work a method for using LES to generate wind velocity fields for the use of autonomous quadrotor or flight was shown. The urban environment is divided into simple geometries to allow for simulating on a desired scale and the ability to build up a larger city sized environments. The one equation LES model is used to resolve the flow around a single building in isolation. Verification and validation of the numerical results is performed by studying the flow on three different grids, using an index quality based on the resolved turbulent kinetic energy and comparing velocity profiles with experimental wind tunnel data. An appropriate loop interval is found and stored in a database and queried by a flight simulator as needed. Two position hold missions are performed to test the controller's ability to maintain satisfactory position control. It is found that the LES generated wind has a larger affect on the deviations away from the desired position than the RANS based wind, up to a 135% radial increase, and even resulted in loss of control and contact with the building. Future work is planned to expand the database of wake simulations to include urban canyons and flows with wind incidence angles to develop improved position controlling methods.

## References

- [1] Urban development, 2014. <http://data.worldbank.org/topic/urban-development>.
- [2] Douglas Murphy and James Cycon. *Applications for mini VTOL UAV for law enforcement*.
- [3] Tamir Hegazy, Ben Ludington, and George Vachtsevanos. Reconnaissance and surveillance in urban terrain with unmanned aerial vehicles. In *Proceedings of 16 th IFAC World Congress*, pages 4–8, 2005.
- [4] Robert D. Miller. Unmanned aerial vehicles: Improving warfighting capabilities in the urban environment. Technical report, DTIC Document, 1998.
- [5] Rodrigo L. Mota, Luiz F. Felizardo, Elcio H. Shiguemori, Alexandre C. Ramos, and Felix Mora-Camino. Expanding small UAV capabilities with ANN: A case study for urban areas inspection. *British Journal of Applied Science & Technology*, 4(2):387–398, 2014.
- [6] Jason Etele. Overview of wind gust modelling with application to autonomous low-level UAV control. DRDC contract report, November 2006.
- [7] W. Rodi. Comparison of LES and RANS calculations of the flow around bluff bodies. *Journal of Wind Engineering and Industrial Aerodynamics*, 69-71:55–75, July 1997.
- [8] P. Gousseau, B. Blocken, and G.J.F. van Heijst. CFD simulation of pollutant dispersion around isolated buildings: On the role of convective and turbulent mass fluxes in the prediction accuracy. *Journal of Hazardous Materials*, 194:422–434, October 2011.
- [9] Tetsuro Tamura. Large eddy simulation on building aerodynamics. In *Proceedings of the seventh Asia-Pacific Conference on Wind Engineering*, pp131-157, 2009.
- [10] Jianming He and Charles C. S Song. Evaluation of pedestrian winds in urban area by numerical approach. *Journal of Wind Engineering and Industrial Aerodynamics*, 81(1-3):295–309, May 1999.
- [11] David Galway, Jason Etele, and Giovanni Fusina. *Urban Wind Modeling with Application to Autonomous Flight*. Masters thesis, Carleton University, February 2009.
- [12] David Galway, J. Etele, and Giovanni Fusina.

- Development and implementation of an urban wind field database for aircraft flight simulation. *Journal of Wind Engineering and Industrial Aerodynamics*, 103:73–85, April 2012.
- [13] David Galway, J. Etele, and Giovanni Fusina. Modeling of urban wind field effects on unmanned rotorcraft flight. *Journal of Aircraft*, 48(5):1613–1620, September 2011.
- [14] Saddok Houda, Noureddine Zemmouri, Abdelmalek Hasseine, Rachid Athmani, and Rafik Belarbi. A CFD model for simulating urban flow in complex morphological street network. *The Online Journal of Science and Technology*, 2(1):1–10, January 2012.
- [15] R. E. Britter and S. R. Hanna. Flow and dispersion in urban areas. *Annual Review of Fluid Mechanics*, 35(1):469–496, 2003.
- [16] Stephen B. Pope. *Turbulent Flows*. Cambridge University Press, August 2000.
- [17] H. Versteeg and W. Malalasekera. *An Introduction to Computational Fluid Dynamics: The Finite Volume Method*. Prentice Hall, Harlow, England ; New York, 2 edition edition, January 2007.
- [18] Eugene de Villers. *The Potential of Large Eddy Simulation for the Modeling of Wall Bounded Flows*. PhD thesis, Imperial College of Science, Technology and Medicine, July 2006.
- [19] Sinisa Krajnovic and Lars Davidson. Large-eddy simulation of the flow around a bluff body. *AIAA Journal*, 40(5):927–936, 2002.
- [20] Jorg Franke, Antti Hellsten, Heinke Schlunzen, and Bertrand Carissimo, editors. *Proceedings / International Workshop on Quality Assurance of Microscale Meteorological Models Cost action 732 in combination with the European Science Foundation at Hamburg, Germany, July 28/29, 2005*. Univ., Meteorological Inst., Centre for Marine and Atmospheric Sciences, Hamburg, 2005.
- [21] Yoshihide Tominaga, Akashi Mochida, Ryuichiro Yoshie, Hiroto Kataoka, Tsuyoshi Nozu, Masaru Yoshikawa, and Taichi Shirasawa. AIJ guidelines for practical applications of CFD to pedestrian wind environment around buildings. *Journal of Wind Engineering and Industrial Aerodynamics*, 96(10-11):1749–1761, October 2008.
- [22] T Meng and K Hibi. Turbulent measurements of the flow field around a high-rise building. *Journal of Wind Engineering Japan*, (76):55–64, 1998. (in Japanese).
- [23] Farzad Bazdidi-Tehrani, Ahmad Ghafouri, and Mohammad Jadidi. Grid resolution assessment in large eddy simulation of dispersion around an isolated cubic building. *Journal of Wind Engineering and Industrial Aerodynamics*, 121:1–15, October 2013.
- [24] I. B. Celik, Z. N. Cehreli, and I. Yavuz. Index of resolution quality for large eddy simulations. *Journal of Fluids Engineering*, 127(5):949–958, September 2005.
- [25] Syed Ali Raza and Jason Etele. Simulation tool for testing and validating uav autopilots in wind gust environments. *AIAA Atmospheric Flight Mechanics Conference and Exhibit*, August 13-16 2012.
- [26] Canadian city data metrics from environment canada, January 2014. [http://toronto.weatherstats.ca/charts/wind\\_speed-5years.html](http://toronto.weatherstats.ca/charts/wind_speed-5years.html).

## 10 Contact Author Email Address

mailto:MarkSutherland@cmail.carleton.ca

## Copyright Statement

The authors confirm that they, and/or their company or organization, hold copyright on all of the original material included in this paper. The authors also confirm that they have obtained permission, from the copyright holder of any third party material included in this paper, to publish it as part of their paper. The authors confirm that they give permission, or have obtained permission from the copyright holder of this paper, for the publication and distribution of this paper as part of the ICAS 2014 proceedings or as individual off-prints from the proceedings.